analytical chemistry

Article

pubs.acs.org/ac

A DNA Tetrahedron Nanoprobe with Controlled Distance of Dyes for Multiple Detection in Living Cells and in Vivo

Na Li,[†] Meimei Wang,[†] Xiaonan Gao, Zhengze Yu, Wei Pan, Hongyu Wang, and Bo Tang*

College of Chemistry, Chemical Engineering and Materials Science, Collaborative Innovation Center of Functionalized Probes for Chemical Imaging in Universities of Shandong, Key Laboratory of Molecular and Nano Probes, Ministry of Education, Institute of Molecular and Nano Science, Shandong Normal University, Jinan 250014, P. R. China

Supporting Information

ABSTRACT: Multicomponent quantitative detection in living samples is becoming increasingly important; however, the current detection strategy may cause fluorescence self-quenching and reduce the sensitivity of detection. To solve the problem, we develop a DNA tetrahedral nanoprobe to control the dyes distance for simultaneous detection of multiple analytes. Compared to mesoporous silica nanoparticles based nanoprobes, the DNA tetrahedral nanoprobes display enhanced fluorescence intensities due to partially avoiding the fluorescence resonance energy transfer. Confocal fluorescence images show that the nanoprobes are capable of detecting and visualizing pH and $O_2^{\bullet-}$ in living cells under a single wavelength excitation. In an inflammation model for mice, the nanoprobes simultaneously image the down-regulation of pH and up-regulation of $O_2^{\bullet-}$. We expect that the current strategy can provide new opportunities in designing probes for multiplexed detection with reduced self-quenching and enhanced sensitivity.

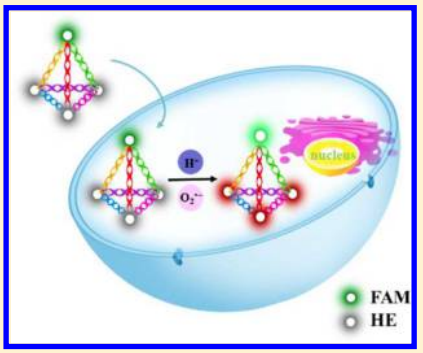

Cellular small molecules, such as metal ions, hydrogen ions, reactive oxygen species, and reactive nitrogen species, play important roles in a variety of physiological and pathological processes.[1−4] These small molecules are concomitantly produced and closely interrelated in whole cell signaling network. Recently, more and more attention has been paid to detect these molecules due to their significant roles in cell signaling pathways.[5] Simultaneous detection of multiple molecules, especially the detection of a variety of small molecules at the same location is of great importance for investigating the cell signaling pathways and the diagnosis of diseases. Molecular probes, as one of the developing nanoprobes, are limited by their active sites and size for such applications.[6] The nanoprobes with the function of assembling a variety of recognition molecules for multiplexed detection become particularly necessary. Mesoporous silica nanoparticles (MSNs)-based nanoprobes,[7−10] which can be loaded with different dyes and transformed into the cells, have been widely employed to determine multiple kinds of small molecules. Since the dyes' distance in the MSNs is too close, the fluorescence self-quenching leads to the decrease of detection sensitivity and imaging clarity. Therefore, the development of new platforms with controllable distance for detection of multiple analytes is urgently required.

In recent years, DNA nanoparticles have attracted great attention owing to excellent biocompatibility and programmability, which can be assembled with well-defined structure and uniform size.[11−14] DNA tetrahedron nanostructure is one of the most widely used structures in biological and medical applications.[15−19] The DNA tetrahedron could be quickly synthesized by four designed isometric single strands with six double-stranded edges and four vertexes. Each vertex of the DNA tetrahedron can modify with different small molecules by covalent interactions. Hence, the DNA tetrahedron-based nanoprobe is expected to simultaneously monitor and image multiple reactive small molecules without self-quenching by accurate control the distance of dye molecules.

In this regard, we develop a new DNA tetrahedral nanoprobe to simultaneously determine pH and superoxide anion ($O_2^{\bullet-}$) with a single wavelength excitation in living cells and in vivo. $O_2^{\bullet-}$, a major precursor of most ROS, is formed by one-electron reduction of the triplet dioxygen molecule. In the presence of hydrogen ions (H^+), the dismutation of $O_2^{\bullet-}$ generates hydrogen peroxide (H_2O_2) and further reduced to hydroxyl radical ($^{\bullet}OH$) or water. Abnormal production of H^+ and $O_2^{\bullet-}$ have been implicated in the inducement and growth of various diseases including inflammation, ischemia-reperfusion injury, neurodegenerative diseases, and cancer.[20] Fluorescein and hydroethidine (HE)[21] as the pH and $O_2^{\bullet-}$ responsive units were conjugated with the vertexes of the tetrahedron, respectively. The DNA tetrahedral nanostructure functionalized with fluorophores can avoid dyes self-quenching compare to the mesoporous silica-based nanoprobes owing to controllable distance of the DNA tetrahedron. The designed nanoprobes are capable of detecting pH and $O_2^{\bullet-}$ in living cells and in vivo with high sensitivity and image resolution, which leads to versatile functions in future chemical sensing and

Received: March 10, 2017
Accepted: May 24, 2017
Published: May 24, 2017

DOI: 10.1021/acs.analchem.7b00889
Anal. Chem. 2017, 89, 6670−6677

imaging applications for low concentration levels of multicomponent in vivo. The details are shown in Scheme 1.

Scheme 1. Illustration of the Nanoprobes for Imaging of Intercellular $O_2^{\bullet-}$ and pH

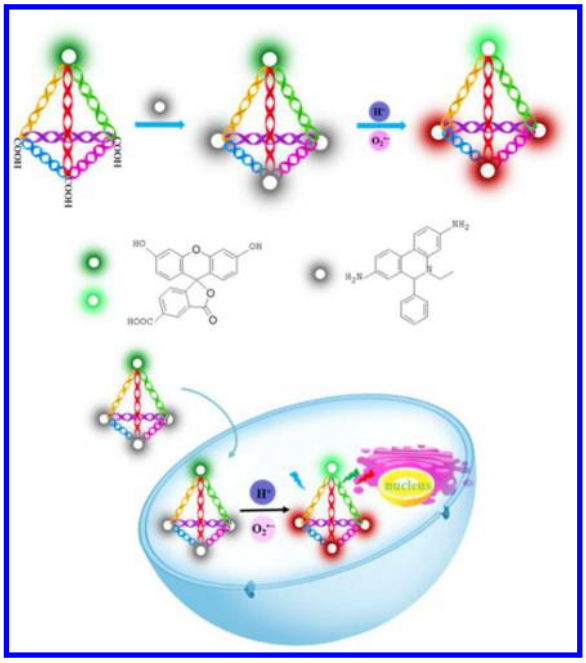

EXPERIMENTAL SECTION

Materials. All DNA sequences used in this work were purchased through Sangon Biotechnology Co., Ltd. (Shanghai, China) and purified by high-performance liquid chromatography (HPLC). HE was purchased from Aladdin. 1-Ethyl-3-(3-(dimethylaminopropyl) carbodiimide hydrochloride (EDC) was purchased from Alfa Aesar Chemical Ltd. (Tianjin, China). Hydrogen peroxide (H_2O_2, 30%), sodium hypochlorite (NaClO, 5.2%), tetramethyl orthosilicate (TMOS), hexadecyl trimethyl ammonium bromide (CTAB), ammonium hydroxide aqueous solution ($NH_3{\cdot}H_2O$) *tert*-butylhydroperoxide (TBHP) were purchased from Sinopharm (Shanghai, China). Xanthine (XA), xanthine oxidase (XO), glutathione (GSH), phorbol 12-myristate 13-acetate (PMA), lipopolysaccharide (LPS), and 3-(4,5-dimethylthiazol-2-yl)-2,5-diphenyltetrazolium bromide (MTT) were obtained from Sigma-Aldrich. 4,5-Dihydroxy-1,3-benzenedisulfonic acid disodium salt (Tiron) was obtained from Shanghai Reagent Co., Ltd. (Shanghai, China). Methoxy-terminated poly(ethylene glycol) (PEG-silane, molecular weight 550) was purchased from Ponsure Biotechnology. Deoxyribonuclease I (DNase I) was purchased from Solarbio Science and Technology Co., Ltd. (Beijing, China). Exonuclease III (Exo III), fluorescein (FAM) was obtained from Thermo Scientific (Shanghai, China). L-012 was purchased from Wako Chemical. Cervical cancer cell line HeLa was obtained from the Committee on Type Culture Collection of Chinese Academy of Sciences. All the chemicals were analytical grade, and ultrapure water with a resistivity of 18.2 MΩ cm was used in all experiments.

Instruments. High-resolution transmission electron microscopy (HRTEM) was carried out on a JEM-2100F electron microscope. Atomic force microscopy (AFM) was performed with Dimension Icon (Bruker Inc.). Fluorescence spectra were measured on an FLS-980 Edinburgh fluorescence spectrometer with a xenon lamp. All pH measurements were performed with a pH-3c digital pH-meter (Shanghai LeiCi Device Works, Shanghai, China) with a combined glass-calomel electrode. Absorbance was obtained in a microplate reader (Synergy 2, Biotek) in the MTT assay. Gel image was measured on JS-680D automatic gel imaging analyzer (Shanghai, China). Confocal fluorescence imaging was performed with a LSM 880 confocal laser scanning microscopy (Zeiss Co., Ltd., Germany) with an objective lens (×20). Flow cytomety analysis was performed with ImageStream^X Mark II. In vivo imaging was obtained from IVIS Lumina III system (Xenogen) with a metal halide lamp (150 W).

Preparation of DNA Tetrahedron-Based Nanoprobes. A two-step synthesis method was carried out to obtain the nanoprobes. The first step was self-assembly of DNA tetrahedron with fluorophore. DNA tetrahedron was synthesized according to the approach reported[22] with minor modifications. Four constituent oligonucleotide strands (P1, P2, P3, and P4) were dissolved and mixed in equimolar in TM buffer (20 mM Tris, 50 mM $MgCl_2$, pH 8.0). The mixed solution was heated to 95 °C for 3 min and then quickly cooled in an ice bath for 5 min. The tetrahedron solution was stored at 4 °C at least 6 h. For the next step, HE was conjugated to as-synthesized DNA tetrahedron by amido bond formation. As-synthesized DNA tetrahedron (0.33 μM) was mixed with EDC (10 μM) and stirred for 30 min to activate the carboxylic group in PBS buffer (pH 7.4) under dark conditions. Subsequently, HE (1 μM) was added to the above solution under stirring for 12 h. The nanoprobe complex was purified by centrifugation at 12000 rpm for 5 min by ultrafiltration devices (30k, 0.5 mL). The as-synthesized nanoprobes were stored at 4 °C for the following experiments. In addition, the nanoprobes of different lengths of DNA strands also were synthesized. Two other nanoprobes with different edge lengths (7 base pair (bp), 10 bp) were synthesized by the same method described above. The nanoprobes used were 17 bp in this paper.

The nanoprobes were characterized by nondenaturing polyacrylamide gels electrophoresis (PAGE), HRTEM and AFM. PAGE (6%) was carried out in 1× TBE buffer (tris borate-EDTA) with 95 V for 1.5 h. Then the gel was stained with 4S Green Plus Nucleic Acid Stain for 15 min and processed by gel imaging analyzer. HRTEM was applied to characterize the morphology of the DNA tetrahedron. For the sample preparation, the solution was dropped on a carbon-coated TEM grid and negatively stained with phosphotungstic acid. The AFM characterization of the DNA tetrahedron nanostructure was carried on freshly cleaved mica.

As a control experiment, MSNs (6.6 nm) were prepared according to the previously reported protocol.[23] CTAB (0.06 mmol) and $NH_3{\cdot}H_2O$ (0.02 M) were added in 8 mL of water. The solution was stirred at 30 °C for 30 min until CTAB fully dissolved. Afterward, 0.11 mmol of TMOS was slowly added under vigorous stirring, and the solution was heated for 24 h. Then PEG-silane (0.21 mmol) was added, and the mixture was further stirred at 30 °C for 24 h. In the next step, the temperature was increased from 30 to 80 °C and the solution was stirred at 80 °C for another 24 h. Then the mixture was cooled to room temperature and purified in the dialysis tube in 100 mL of acid solution (water, ethanol, and acetic acid = 1:1:0.007) for 24 h to extract CTAB out of the pores of the particles. This process was repeated 3 times. The solution was then dialyzed in 2000 mL of water for another 24 h and the

DOI: 10.1021/acs.analchem.7b00889
Anal. Chem. 2017, 89, 6670−6677

process was repeated 3 times. After the purification, MSNs were added into a mixture solution of FAM and HE under stirring for 12 h. The amounts of FAM and HE in the MSNs were regulated the same as in the tetrahedron.

General Procedure for Fluorescence Determination. In order to test the response of the nanoprobes to pH, different pH standard buffer solutions were made by mixing 10 mM Na_2HPO_4 and 10 mM NaH_2PO_4 at varied volume ratios. The accurate pH values were determined by a pH-3c digital pH-meter. Such a series of standard pH buffer solutions mixed with as-synthesized nanoprobes and the fluorescence intensity was measured at λex/λem = 488 nm/515 nm. In order to test the response of $O_2^{\bullet-}$, the XO/XA system was performed to generate $O_2^{\bullet-}$ in PBS buffer. One unit XO can catalyze 1 mol of XA to come into 0.33 mol $O_2^{\bullet-}$. The nanoprobes mixed with various concentrations of XO/XA and were incubated at 37 °C for 30 min. The fluorescence intensity was measured at λex/λem = 488 nm/580 nm. The fluorescence intensity of MSNs-FAM-HE proceeded under the same conditions.

Various intracellular substances were selected to evaluate the effect of the nanoprobes to H^+, including metal ions Na^+, K^+, Mg^{2+}, Mn^{2+}, Zn^{2+}, Ca^{2+}, Fe^{2+}, Fe^{3+}, and Co^{2+}. H_2O_2 and GSH, which are the intracellular oxidative-stress-associated redox chemicals, were also tested. In addition, certain kinds of amino acids His, Lys, Arg, Try, Cys, Hcy were applied to the test. Reactive oxygen species, reactive nitrogen species and other biological compounds (NaClO, $^1O_2$, $^{\bullet}OH$, H_2O_2, TBHP, NO, $ONOO^-$, GSH, VC) were used to evaluate the effect of the nanoprobes to $O_2^{\bullet-}$.

Stability of the Nanoprobes. The stability of the nanoprobes under cell culture medium and continuous light illumination was investigated. The nanoprobes were dissolved in cell culture medium and excited at 488 nm at different times. To evaluate the stability of the nanoprobes under continuous light illumination, the fluorescence kinetics of FAM and HE were conducted by a fluorescence spectrometer with a xenon lamp. In order to demonstrate nuclease stability of the nanoprobes, DNase I (1 U/mL) and Exo III (1 U/mL) were incubated with the tetrahedron at 37 °C for various time including 2, 4, 8, 12, or 24 h, respectively. Then, the mixtures were run in 1× TBE buffer at 95 V for 1.5 h by PAGE.

Cell Culture and Cytotoxicity Assay. HeLa cells were cultured in Dulbecco's modified Eagles medium (DMEM) supplemented with 10% fetal bovine serum and 100 U/mL of 1% antibiotics penicillin/streptomycin and maintained at 37 °C in a 100% humidified atmosphere containing 5% CO_2/95% air incubator MCO-15AC. Standard MTT assay was applied to evaluate cytotoxicity of the nanoprobes. HeLa cells (1×10^6 cells/well) were cultured in 96-well microtiter plates at 37 °C for 24 h. After the removal of initial medium, the cells were incubated with three different concentrations of the nanoprobes (0.15 μM, 0.33 μM, 0.50 μM) for 4, 8, and 12 h each. Then a volume of 200 μL/well MTT (0.5 mg/mL) solution was added. After 4 h, the MTT solutions were removed and 150 μL of DMSO was added in order to dissolve the formazan crystals. The absorbance was measured at 490 nm for 3 times to show as the mean ± SD.

Intracellular Confocal Fluorescence Imaging. HeLa cells were plated on chamber slides for 24 h before imaging assay. Then the nanoprobes (0.33 μM) dissolved in DMEM were incubated with the cells for 4 h at 37 °C. Before imaging, the cells on chamber slides were washed 3 times with PBS (pH = 7.4) buffer to remove the nanoprobes that were not uptaken by the cells. To monitor the ability of the nanoprobes for testing intracellular pH, the nanoprobes-loaded cells were incubated at 37 °C for 30 min in high K^+ buffer (1 mM $CaCl_2$, 0.5 mM $MgSO_4$, 30 mM NaCl, 120 mM KCl, 1 mM NaH_2PO_4, 5 mM glucose, 20 mM HEPES) with various pH values in the presence of 10 μM nigericin before imaging. The intracellular imaging was obtained by confocal laser scanning microscopy with 488 nm excitation and emission filter at 500−540 nm (green channel). In order to evaluate the amount of intracellular $O_2^{\bullet-}$, exogenous $O_2^{\bullet-}$ was also generated from XA/XO and the sample was further incubated for 30 min. To simultaneously monitor the pH and $O_2^{\bullet-}$changes in living cells, three groups experiment were carried out: the cells incubated with the nanoprobes were taken as the control group; the other two groups were incubated with PMA (1.0 μg/mL) for 30 min before incubation with the nanoprobes. One group of PMA-stimulated cells were incubated again with Tiron (10 μM) for 30 min. Confocal fluorescence imaging was captured with 488 nm excitation and emission at 560−630 nm (red channel) and 500−540 nm (green channel). The confocal fluorescence images of MSNs-FAM-HE were proceeded under the same conditions. All background parameters (the laser intensity, exposure time, objective lens) were fixed when the different fluorescence images were measured.

Flow Cytometry. HeLa cells were seeded on cell culture dishes for 24 h. Then the nanoprobes dissolved in DMEM were incubated with the cells for 4 h at 37 °C. The treating process of different pH and $O_2^{\bullet-}$ was consistent with confocal fluorescence imaging. Trypsin was added to each culture dish and incubated for 1 min. Then, DMEM was added and the cells were washed 3 times by PBS. Finally, the cells were analyzed by flow cytometry. The excitation wavelength is 488 nm and the emission wavelength was collected in the range of 500−540 nm and 560−630 nm.

In Vivo Fluorescence Imaging. All animal experiments were carried out and accorded with the Principles of Laboratory Animal Care (People's Republic of China). Female nude mice (4−6 weeks old, ∼20 g) were given an intraperitoneal injection of LPS (2.5 mg/mL in saline) to induce serious inflammation. After 4 h, the mice were intraperitoneally injected the nanoprobes' solution (10 μM, 0.10 mL). Meanwhile, mice treated with LPS and injected with the nanoprobes at the same region as negative control were prepared. The mice were anesthetized by an intraperitoneal injection of 4% chloral hydrate (0.10 mL). Images were obtained (20 min after injected of the nanoprobes) by the IVIS Lumina III system with a 480 nm excitation filter, and emission was collected at 500−540 nm (FAM channel) and 580−620 nm (HE channel). The L-012 probe (75 mg/kg) was intraperitoneally injected. The image exposure time was 15 s, blocked excitation filter, and open emission filter.

RESULTS AND DISCUSSION

Design and Synthesis of the Nanoprobes. To accomplish the detection of intracellular pH and $O_2^{\bullet-}$, the nanoprobes were fabricated as follows. First, three DNA single strands (P1, P2, and P3) modified with carboxyl groups and the P4 modified with the FAM were mixed in equimolar amounts to construct the DNA tetrahedron via the annealing process (Table S1 for detailed sequences). FAM, which performs as a pH-sensitive fluorophore, is connected to one vertex of the tetrahedron to monitor pH changes with an emission peak at 515 nm. Further, HE, an $O_2^{\bullet-}$ sensitive fluorophore, was

DOI: 10.1021/acs.analchem.7b00889
Anal. Chem. 2017, 89, 6670−6677

conjugated on the other three vertices of tetrahedron by the coupling effect of EDC. Although HE is weakly fluorescent by itself, it exhibits enhanced fluorescence intensity at 580 nm after specifically response to $O_2^{\bullet-}$. The dye molecules FAM and HE were available on the four vertices of the DNA tetrahedron to achieve simultaneous determination of pH and $O_2^{\bullet-}$. As HE and FAM possess a single-wavelength excitation at 488 nm but various emission wavelengths at 515 and 580 nm (Figure S1), it leads to effectively avoid intricate manipulation and spectral overlap from multiple excitations.

Characterizations of the Nanoprobes. In order to determine the synthesis process of the nanoprobes, native polyacrylamide gel electrophoresis (PAGE) was applied for identifying their electrophoretic mobility. In Figure 1A, as the number of DNA strands increases from P1 to P4, the DNA tetrahedral bands migrated more slowly than other DNA combinations. However, the band of the nanoprobes in lane 5 has no obvious change due to the conjugation of HE with the tetrahedron. The clear band verifies the success of self-assembly process of tetrahedron. The formation of DNA tetrahedron was further proved by HRTEM (Figure 1B) and AFM (Figure 1C). AFM demonstrates the tetrahedral morphology and the size well matches with HRTEM results. Moreover, Figure S2 indicates the size and height distribution of the DNA tetrahedron. A mean diameter of the tetrahedron is approximately 6.0 ± 1.0 nm, which is consistent with the theoretical edge length of the DNA tetrahedron (5.8 nm).[24] These results indicate the successful synthesis of as designed DNA tetrahedron and the nanoprobes.

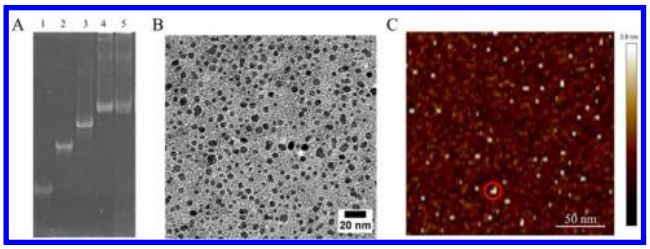

Figure 1. (A) PAGE imaging (6%) was used to verify formation of the nanoprobes. Lane 1, P1; Lane 2, P1 + P2; Lane 3, P1 + P2 + P3; Lane 4, P1 + P2 + P3 + P4; Lane 5, the nanoprobes. (B) HRTEM image of the DNA tetrahedron. Scale bar is 20 nm. (C) Characterization of DNA tetrahedron with AFM. Scale bar is 50 nm.

To confirm the stability of the nanoprobes as an effective imaging agent, we evaluated the fluorescence variation of the nanoprobes under cell culture medium and continuous light illumination. As shown in Figure S3, the fluorescence intensity was stable after the nanoprobes dissolved in DMEM for 12 h. The fluorescence kinetics of FAM and HE were carried out to prove the stability of the nanoprobes under continuous light illumination. As shown in Figure S4, the fluorescence emission intensity was still stable after 60 min of light illumination. The results show that the nanoprobes are stable in the process of detection and imaging of aqueous solution and cell.

Responses of the Nanoprobes to pH and $O_2^{\bullet-}$. For a comparison study, MSNs-based nanoprobes were applied to monitor the responses toward pH and $O_2^{\bullet-}$, separately. In Figure S5, the fluorescence intensity of MSNs-FAM-HE to different pH was lower than the tetrahedron-based nanoprobes. In Figure S6, the fluorescence response of MSNs-FAM-HE to $O_2^{\bullet-}$ (2 μM) was about 2-fold, while the nanoprobes to equal amount of $O_2^{\bullet-}$ was 6-fold. The results show that DNA tetrahedral nanoprobes show more enhanced fluorescence intensity. It can be explained that FAM and HE, after being loaded into MSNs, exist at a certain degree of self-quenching due to close intermolecular distance. However, the DNA tetrahedron can control exact distance of FAM and HE at the vertices due to the fixed edge length, which significantly reduced fluorescence resonance energy transfer, so it partially avoids the fluorescence self-quenching effect compared to MSNs-FAM-HE. Therefore, the as-synthesized nanoprobes based on the DNA tetrahedron are favorable for monitoring pH and $O_2^{\bullet-}$. Meantime, to demonstrate the role of the length of the DNA sequence, the nanoprobes with different edge lengths DNA tetrahedron were synthesized (Table S2 for detailed sequences). As shown in Figure S7, the fluorescence responses of three kinds of nanoprobes (7 bp, 10 bp, 17 bp) to $O_2^{\bullet-}$ (2 μM) were 3.7-fold, 4.2-fold, 6-fold, respectively. Because HE is connected to the three vertices of the DNA tetrahedron, the distance between HE increases with the increase of the length of the DNA strand. Therefore, the self-quenching effect of the nanoprobes decline gradually with the increase of the edge lengths of DNA tetrahedron.

Next, the response of the nanoprobes to pH and $O_2^{\bullet-}$ were carried out. The fluorescence responses of the nanoprobes for various pH values are shown in Figure 2A: as pH changes from acidic to basic (6.0–8.3), the emission intensities at 515 nm for FAM increase gradually while the emission at 580 nm for the oxidation products of HE changes quite mildly under a single excitation 488 nm. Fluorescence intensity linearly correlates with pH values in the range of 6.0–8.3 (Figure 2B) and the correlation coefficient is 0.9962. Meanwhile, the fluorescence responses of the nanoprobes for $O_2^{\bullet-}$ are shown in Figure 2C: with an increasing concentrations of $O_2^{\bullet-}$ from 0 to 2 μM, the emission intensity at 580 nm increases significantly while the intensity change at 515 nm is negligible. Moreover, the linear correlation coefficient between fluorescence intensity and concentrations of $O_2^{\bullet-}$ is 0.9959 (Figure 2D) with the detection limit of 7.2 nM,[25] much lower compared to previous reported MSNs-based nanoprobes[26,27] and other reported $O_2^{\bullet-}$

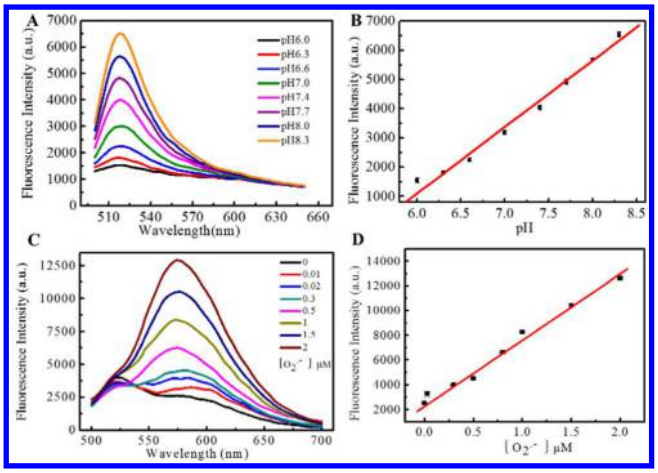

Figure 2. (A) Fluorescence emission spectra (λex = 488 nm) of the nanoprobes with various pH values from 6.0 to 8.3. (B) Linear relationship between the fluorescence intensity and pH values. (C) Fluorescence emission spectra (λex = 488 nm) of the nanoprobes with various concentrations of $O_2^{\bullet-}$ (0–2 μM, incubated by XO/XA for 30 min at 37 °C). (D) Linear relationship between the fluorescence intensity and $O_2^{\bullet-}$ concentrations.

DOI: 10.1021/acs.analchem.7b00889
Anal. Chem. 2017, 89, 6670–6677

fluorescent probes.[28,29] HE was connected at the three vertexes of the tetrahedron, which greatly decreased the effect of self-quenching. Considering the low concentration, short lifetime, and high reactivity of $O_2^{\bullet-}$ in the living cell, the lower detection limit to the detection of $O_2^{\bullet-}$ is more helpful, so the as-synthesized nanoprobes provide a promising approach for monitoring of $O_2^{\bullet-}$. The above results indicate that the designed nanoprobes enable separate or concurrent detection of pH values and $O_2^{\bullet-}$ without mutual interference.

Selectivity of the Nanoprobes toward pH and $O_2^{\bullet-}$. Because of the complicated components of living cells, selectivity is also a very key factor for analytical applications. To evaluate the selectivity of the nanoprobes to pH, potential interferences including 9 kinds of metal ions (Na^+, K^+, Mg^{2+}, Mn^{2+}, Zn^{2+}, Ca^{2+}, Fe^{2+}, Fe^{3+}, Co^{2+}), glutathione (GSH), H_2O_2, and multiamino acids (His, Lys, Arg, Try, Cys, Hcy) that coexist in the living cells were examined in parallel under the same conditions. No obvious fluorescence change was observed for multimetallic ions and redox and amino acids (Figure S8) indicating that the presence of these substances has no obvious effect to pH detection of the nanoprobes. Meanwhile, the selectivity of the nanoprobes to $O_2^{\bullet-}$ was also investigated: different interfering agents, including NaClO, $^1O_2$, $^\bullet OH$, H_2O_2, TBHP, NO, $ONOO^-$, GSH, and VC were performed. The nanoprobes display significant selectivity to $O_2^{\bullet-}$ over other ROS and reductants (Figure S9). Overall, the results validated that the nanoprobes can monitor pH and $O_2^{\bullet-}$ without other common interferences in living cells.

Enzymatic Resistance of the Nanoprobes. Nuclease resistance of the nanoprobes is quite important for an imaging application in living cells. To examine nuclease stability of the nanoprobes, two kinds of commonly used nucleases, DNase I and Exo III were utilized to incubate with DNA tetrahedron. DNase I is an important enzyme that nonspecifically degrades single and double stranded DNA molecules into small fragments by cleaving the phosphodiester bonds in the DNA backbone.[30] Exo III is a 3′ → 5′ exonuclease, hydrolyzing 3′-hydroxyl-terminated phosphomonoesters of duplex DNA.[31] The DNA tetrahedron was treated with DNase I (1 U/mL) and Exo III (1 U/mL) at 37 °C with different time periods. PAGE shows the tetrahedron bands remained clear within 4 h incubation with DNase I and Exo III, illustrating the resistance of nanostructure to degradation of endo- and exonucleases (Figure 3). With the increase of incubation time, the bands were slowly weakening. However, observed attenuated bands with enhanced incubation times to 24 h reveals the partial existence of the nanostructure. The resistance contributes to the steric hindrance of the DNA tetrahedron nanostructure leading to declined binding of enzymes to DNA. Therefore, the 3D-tetrahedron structure can resist specific and nonspecific nucleases,[14,15,31] which makes it useful as a promising substrate for transporting other materials. Moreover, compared to other nanomaterials, such as metal semiconductor materials and silicon nanomaterials which are not biodegradable or potentially toxic to cells, the DNA nanostructure is excellent in biodegradation and nontoxic as an imaging vector.

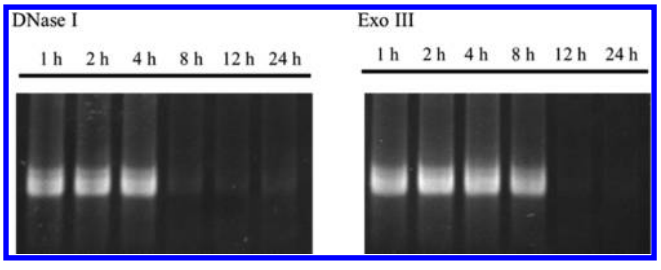

Figure 3. Electrophoretic analysis of the DNA tetrahedron of nuclease stability in the presence of DNase I (1 U/mL) or Exo III (1 U/mL) at 37 °C under various times by using PAGE.

Cell Cytotoxicity Assay. In order to further apply the nanoprobes into biological experiments, cytotoxicity of the nanoprobes was also evaluated by a MTT assay.[32] The absorbance of MTT at 490 nm relies on the activation degree of cells, and the cell viability of the control group was about 100%. Figure S10 shows that the viability of cells keeps more than 90% after the nanoprobes incubated with cells for different time periods (4, 8, and 12 h) under different concentrations. It reveals that the nanoprobes have no side effects on the living cell detection although 2-fold higher concentration than that used in the following experiments. High cell viability of the nanoprobes indicated that it can be applied to intracellular detection of pH and $O_2^{\bullet-}$ without cytotoxicity.

Cell Imaging of pH and $O_2^{\bullet-}$ Fluctuations. MSNs-FAM-HE was also used as comparison to image pH and $O_2^{\bullet-}$ in living cells. In order to detect pH, intracellular pH was homogenized by high K^+ buffer of different pH values and ionophore nigericin (10 μM) before imaging. In Figure S11, confocal fluorescence images of MSNs-FAM-HE were much weaker than the nanoprobes under various pH. In Figure S12, confocal fluorescence images of MSNs-FAM-HE exhibit a much weaker intensity compared to the nanoprobes, indicating that the nanoprobes to $O_2^{\bullet-}$ are more sensitive than MSNs-FAM-HE. Moreover, the result is consistent with fluorescence spectra results. Therefore, the nanoprobes are also more suitable for intracellular detection of pH and $O_2^{\bullet-}$.

Then, we employed the nanoprobes to image intracellular pH and $O_2^{\bullet-}$. For intracellular pH imaging, the nanoprobes were incubated with HeLa cells before homogenizing treatment. As shown in Figure 4, the green fluorescence emission

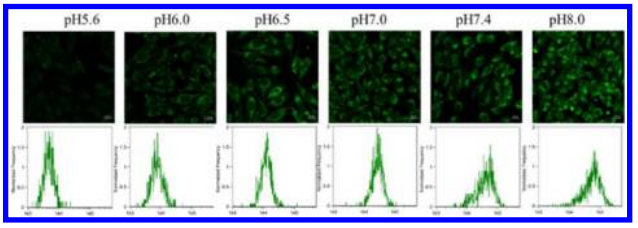

Figure 4. (Top) Confocal fluorescence images of HeLa cells incubated with the nanoprobes at pH 5.6, 6.0, 6.5, 7.0, 7.4, and 8.0, separately. Scale bars are 20 μm. (Bottom) Corresponding flow cytometry analysis of HeLa cells.

intensity of confocal fluorescence imaging and flow cytometry analysis both showed that the fluorescence intensity gradually increased with the increase of pH from 5.6 to 8.0. The results demonstrate the capability of the nanoprobes monitoring and imaging pH changes in living cells. Afterward, HeLa cells were cultured with various concentrations of $O_2^{\bullet-}$ (0, 0.1, 0.5, 1, and 2 μM) for evaluation, and the red fluorescence emission intensities of confocal fluorescence imaging and flow cytometry analysis both showed that the fluorescence intensity successively enhanced with the increasing concentration of $O_2^{\bullet-}$ (Figure 5). Therefore, it can be concluded that the nanoprobes are able to monitor and image intracellular pH and $O_2^{\bullet-}$.

DOI: 10.1021/acs.analchem.7b00889
Anal. Chem. 2017, 89, 6670−6677

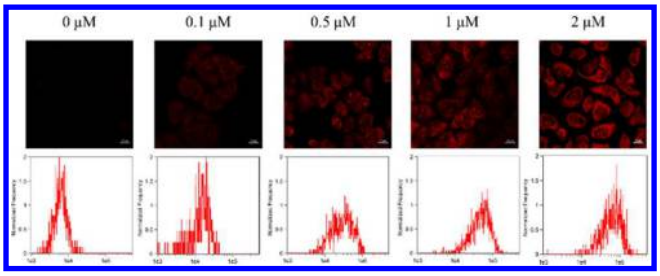

Figure 5. (Top) Confocal fluorescence images of HeLa cells incubated with the nanoprobes with different concentrations of $O_2^{\bullet-}$: 0, 0.1, 0.5, 1, 2 μM, separately. Scale bars are 20 μm. (Bottom) Corresponding flow cytometry analysis of HeLa cells.

The nanoprobes were then applied into living cells for investigating the relationship of pH and $O_2^{\bullet-}$. PMA, a potent stimulus of the respiratory burst, was used to generate excessive $O_2^{\bullet-}$.[33] In Figure 6A, the faint intracellular background

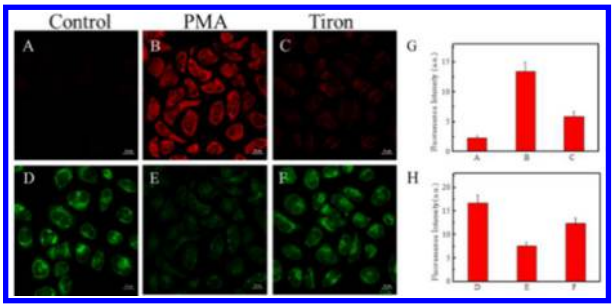

Figure 6. Confocal fluorescence images of HeLa cells. (A, D) Control group. (B, E) HeLa cells stimulated with PMA (1.0 μg/mL) for 30 min before incubation with the nanoprobes. (C, F) HeLa cells stimulated with PMA then treating with Tiron (10 μM) for 30 min. (A–C) The excitation wavelength is 488 nm and the emission wavelength was collected in the range of 560–630 nm. (D–F) The excitation wavelength is 488 nm and the emission wavelength was collected in the range of 500–540 nm. (G, H) Mean fluorescence intensity of the nanoprobes treated cells in panels A–F. Scale bars are 20 μm.

fluorescence was observed after incubating the nanoprobes with HeLa cells. Subsequently, HeLa cells were stimulated to produce $O_2^{\bullet-}$ by PMA in advance, and intense red fluorescence emission was observed in Figure 6B. However, the green fluorescence (Figure 6E) is weaker than the control group (Figure 6D). The results reveal that increasing intracellular concentration of $O_2^{\bullet-}$ caused a decrease of pH. Tiron, as an $O_2^{\bullet-}$ scavenger,[34] was further cultured with PMA stimulated HeLa cells. The red fluorescence intensity became dim in Figure 6C while the green fluorescence intensity of the pH channel (Figure 6F) became stronger than that in Figure 6E. The result is consistent with previous research.[35] In Figure 6G,H, it further proves that the quantitative intensity is corresponding to the results of confocal fluorescence images. Flow cytometry analysis also shows the same result (Figure S13). Therefore, it confirms that the nanoprobes are capable of monitoring intracellular $O_2^{\bullet-}$ variation and simultaneously monitoring the pH change during different processes.

Application of the Nanoprobes in Animal Model. Finally, because of the successful monitoring of the nanoprobes to intracellular pH and $O_2^{\bullet-}$, the feasibility for the detection of pH and $O_2^{\bullet-}$ alterations in vivo was also carried out. The mice abdominal inflammation model caused by LPS was used for in vivo application. Oxidative stress and changed pH are significant features in many inflammatory diseases. Inflammation, as the first response of the immune system, is associated with many diseases such as cancer and atherosclerosis.[36] L-012, a luminescent probe, was applied as a ROS/RNS-sensing probe to detect in vivo inflammation.[37] In Figure S14, the strong chemiluminescence confirmed the successful establishment of the inflammation model. As can be seen in Figures S15 and S16, the nanoprobes do not cause inflammation and histopathological toxicological effects to mice. The nanoprobes were employed via intraperitoneal injection for in vivo relevance of pH/$O_2^{\bullet-}$ in the inflammation process. The mice were divided into three groups: the first group was only injected with LPS in the peritoneal cavity as a control group, whereas the other two groups were treated with the nanoprobes at the same region, one of which suffered skin-pop injection of LPS in advance. The control group emitted almost no fluorescence, suggesting single LPS without the interference to fluorescence intensity (Figure 7A (a), C (a)). However, the

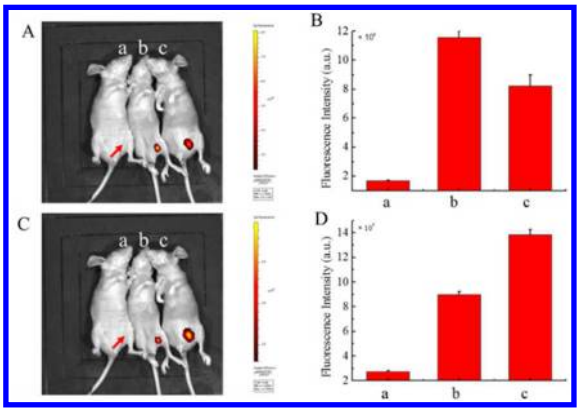

Figure 7. In vivo fluorescence images (pseudo color) of mice in LPS-induced inflammatory model. (a) Only LPS was injected as control. (b) Only the nanoprobes were injected. (c) LPS was intraperitoneal injection and followed to inject the nanoprobes. Red arrow in part A refer to region LPS injected. (A) The excitation filter was 480 nm and emission was collected at 500–540 nm. (C) The excitation filter was 480 nm and emission was collected at 580–620 nm. (B, D) Quantification of fluorescence intensity from parts A and C.

mice injected with both LPS and the nanoprobes showed lower fluorescence intensity than the mice with only the nanoprobes (Figure 7A (b,c)), suggesting an acidification environment in the inflammatory region induced by LPS.[38,39] Moreover, the mice treated with both LPS and the nanoprobes exhibited higher fluorescence intensity than that injection of only the nanoprobes (Figure 7C (b,c)), demonstrating the increase of the $O_2^{\bullet-}$ in the inflammation model. These results exhibit the decrease of pH and the concentration increase of $O_2^{\bullet-}$ in the inflammation induced by LPS, where the quantitative intensity well illustrates the above results (Figure 7B, D). It is assumed that the decrease of pH in inflamed tissues induces dysfunction of cells, which further raises oxidation pressure.[40] All results demonstrate that pH and $O_2^{\bullet-}$ are related during the inflammation process.

CONCLUSIONS

In summary, a DNA tetrahedron-based nanoprobe has been developed for simultaneous detection of pH and $O_2^{\bullet-}$ by avoiding dyes self-quenching in living cells and in vivo.

DOI: 10.1021/acs.analchem.7b00889
Anal. Chem. 2017, 89, 6670–6677

Fluorescein and hydroethidine are modified to four vertices of the tetrahedron, which serve as pH and $O_2^{\bullet-}$ response groups, respectively. The nanoprobes exhibit much higher sensitivity compared with the traditional mesoporous silica-based nanoprobes, since the distance between indicators is fixed which partially reduces the dyes self-quenching. The tetrahedron nanostructure can be uptaken by living cells and exhibits low cytotoxicity and high resistance to enzymatic degradation. Additionally, confocal fluorescence images verify that the nanoprobes have a capacity for dependably describing and selectively discerning the pH and $O_2^{\bullet-}$ in living cells. In the inflammation model in vivo, the nanoprobes simultaneously visualize the down-regulation of pH and up-regulation of $O_2^{\bullet-}$ under a same excitation wavelength. Such nanoprobe develops a new route and design for simultaneous detection of multiple intracellular small molecules with high sensitivity, offering new prospective for future clinical diagnosis and therapy.

■ ASSOCIATED CONTENT

Supporting Information

The Supporting Information is available free of charge on the ACS Publications website at DOI: 10.1021/acs.analchem.7b00889.

DNA sequences, supporting figures of the excitation and emission curves of FAM and HE, the size and height distribution, the stability of the nanoprobes, selectivity, MTT assay, and in vivo imaging results (PDF)

■ AUTHOR INFORMATION

Corresponding Author

*E-mail: tangb@sdnu.edu.cn.

ORCID

Bo Tang: 0000-0002-8712-7025

Author Contributions

†Na Li and Meimei Wang contributed equally to this work.

Notes

The authors declare no competing financial interest.

■ ACKNOWLEDGMENTS

This work was supported by 973 Program (Grant 2013CB933800), the National Natural Science Foundation of China (Grants 21390411, 21535004, 21422505, 21375081, and 21505087), and the Natural Science Foundation for Distinguished Young Scholars of Shandong Province (Grant JQ201503).

■ REFERENCES

(1) Tavassoli, A.; Hamilton, A. D.; Spring, D. R. *Chem. Soc. Rev.* **2011**, *40*, 4269−4270.
(2) Carter, K. P.; Young, A. M.; Palmer, A. E. *Chem. Rev.* **2014**, *114*, 4564−4601.
(3) Shi, W.; Li, X.; Ma, H. *Angew. Chem., Int. Ed.* **2012**, *51*, 6432−6435.
(4) Fialkow, L.; Wang, Y.; Downey, G. P. *Free Radical Biol. Med.* **2007**, *42*, 153−164.
(5) Chen, X.; Tian, X.; Shin, I.; Yoon, J. *Chem. Soc. Rev.* **2011**, *40*, 4783−4804.
(6) Kalyanaraman, B.; Darley-Usmar, V.; Davies, K. J. A.; Dennery, P. A.; Forman, H. J.; Grisham, M. B.; Mann, G. E.; Moore, K.; Roberts, L. J.; Ischiropoulos, H. *Free Radical Biol. Med.* **2012**, *52*, 1−6.
(7) Pan, W.; Wang, H.; Yang, L.; Yu, Z.; Li, N.; Tang, B. *Anal. Chem.* **2016**, *88*, 6743−6748.
(8) Yang, L.; Li, N.; Pan, W.; Yu, Z.; Tang, B. *Anal. Chem.* **2015**, *87*, 3678−3684.
(9) Li, Y.; Zhao, Y.; Chan, W.; Wang, Y.; You, Q.; Liu, C.; Zheng, J.; Li, J.; Yang, S.; Yang, R. *Anal. Chem.* **2015**, *87*, 584−591.
(10) Meng, H.-M.; Jin, Z.; Lv, Y.; Yang, C.; Zhang, X.-B.; Tan, W.; Yu, R.-Q. *Anal. Chem.* **2014**, *86*, 12321−12326.
(11) Pinheiro, A. V.; Han, D.; Shih, W. M.; Yan, H. *Nat. Nanotechnol.* **2011**, *6*, 763−772.
(12) Zhang, F.; Nangreave, J.; Liu, Y.; Yan, H. *J. Am. Chem. Soc.* **2014**, *136*, 11198−11211.
(13) Pei, H.; Zuo, X.; Zhu, D.; Huang, Q.; Fan, C. *Acc. Chem. Res.* **2014**, *47*, 550−559.
(14) Liang, L.; Li, J.; Li, Q.; Huang, Q.; Shi, J.; Yan, H.; Fan, C. *Angew. Chem., Int. Ed.* **2014**, *53*, 7745−7750.
(15) Tay, C. Y.; Yuan, L.; Leong, D. T. *ACS Nano* **2015**, *9*, 5609−5617.
(16) Xie, N.; Huang, J.; Yang, X.; Yang, Y.; Quan, K.; Wang, H.; Ying, L.; Ou, M.; Wang, K. *Chem. Commun.* **2016**, *52*, 2346−2349.
(17) Lee, H.; Lytton-Jean, A. K. R.; Chen, Y.; Love, K. T.; Park, A. I.; Karagiannis, E. D.; Sehgal, A.; Querbes, W.; Zurenko, C. S.; Jayaraman, M.; Peng, C. G.; Charisse, K.; Borodovsky, A.; Manoharan, M.; Donahoe, J. S.; Truelove, J.; Nahrendorf, M.; Langer, R.; Anderson, D. G. *Nat. Nanotechnol.* **2012**, *7*, 389−393.
(18) Li, J.; Hong, C.-Y.; Wu, S.-X.; Liang, H.; Wang, L.-P.; Huang, G.; Chen, X.; Yang, H.-H.; Shangguan, D.; Tan, W. *J. Am. Chem. Soc.* **2015**, *137*, 11210−11213.
(19) Pei, H.; Liang, L.; Yao, G.; Li, J.; Huang, Q.; Fan, C. *Angew. Chem., Int. Ed.* **2012**, *51*, 9020−9024.
(20) Dickinson, B. C.; Chang, C. J. *Nat. Chem. Biol.* **2011**, *7*, 504−511.
(21) Bindokas, V. P.; Jordan, J.; Lee, C. C.; Miller, R. J. *J. Neurosci.* **1996**, *16*, 1324−1336.
(22) Goodman, R. P.; Berry, R. M.; Turberfield, A. J. *Chem. Commun.* **2004**, 1372−1373.
(23) Ma, K.; Sai, H.; Wiesner, U. *J. Am. Chem. Soc.* **2012**, *134*, 13180−13183.
(24) Goodman, R. P.; Heilemann, M.; Doose, S.; Erben, C. M.; Kapanidis, A. N.; Turberfield, A. J. *Nat. Nanotechnol.* **2008**, *3*, 93−96.
(25) Gao, X.; Ding, C.; Zhu, A.; Tian, Y. *Anal. Chem.* **2014**, *86*, 7071−7078.
(26) Huang, H.; Dong, F.; Tian, Y. *Anal. Chem.* **2016**, *88*, 12294−12302.
(27) Zhou, Y.; Ding, J.; Liang, T.; Abdel-Halim, E. S.; Jiang, L.; Zhu, J.-J. *ACS Appl. Mater. Interfaces* **2016**, *8*, 6423−6430.
(28) Gao, X.; Ding, C.; Zhu, A.; Tian, Y. *Anal. Chem.* **2014**, *86*, 7071−7078.
(29) Hu, J. J.; Wong, N. K.; Ye, S.; Chen, X.; Lu, M. Y.; Zhao, A. Q.; Guo, Y.; Ma, A. C. H.; Leung, A. Y. H.; Shen, J.; Yang, D. *J. Am. Chem. Soc.* **2015**, *137*, 6837−6843.
(30) Keum, J.-W.; Bermudez, H. *Chem. Commun.* **2009**, 7036−7038.
(31) Demple, B.; Johnson, A.; Fung, D. *Proc. Natl. Acad. Sci. U. S. A.* **1986**, *83*, 7731−7735.
(32) Luan, M.; Li, N.; Pan, W.; Yang, L.; Yu, Z.; Tang, B. *Chem. Commun.* **2017**, *53*, 356−359.
(33) Oushiki, D.; Kojima, H.; Terai, T.; Arita, M.; Hamnaoka, K.; Urano, Y.; Nagano, T. *J. Am. Chem. Soc.* **2010**, *132*, 2795−2801.
(34) Zhang, W.; Li, P.; Yang, F.; Hu, X.; Sun, C.; Zhang, W.; Chen, D.; Tang, B. *J. Am. Chem. Soc.* **2013**, *135*, 14956−14959.
(35) Chen, Y.; Zhu, C.; Cen, J.; Bai, Y.; He, W.; Guo, Z. *Chem. Sci.* **2015**, *6*, 3187−3194.
(36) Pu, H.-L.; Chiang, W.-L.; Maiti, B.; Liao, Z.-X.; Ho, Y.-C.; Shim, M. S.; Chuang, E.-Y.; Xia, Y.; Sung, H.-W. *ACS Nano* **2014**, *8*, 1213−1221.
(37) Kielland, A.; Blom, T.; Nandakumar, K. S.; Holmdahl, R.; Blomhoff, R.; Carlsen, H. *Free Radical Biol. Med.* **2009**, *47*, 760−766.
(38) Grabowski, J.; Vazquez, D. E.; Costantini, T.; Cauvi, D. M.; Charles, W.; Bickler, S.; Talamini, M. A.; Vega, V. L.; Coimbra, R.; Maio, A. D. *J. Surg. Res.* **2012**, *173*, 127−134.
(39) Okajima, F. *Cell. Signalling* **2013**, *25*, 2263−2271.

DOI: 10.1021/acs.analchem.7b00889
Anal. Chem. 2017, 89, 6670−6677

(40) Trevani, A. S.; Andonegui, G.; Giordano, M.; Lopez, D. H.; Gamberale, R.; Minucci, F.; Geffner, J. R. *J. Immunol.* **1999**, *162*, 4849−4857.

DOI: 10.1021/acs.analchem.7b00889
Anal. Chem. 2017, 89, 6670−6677